DOI 10.1007/s11141-021-10073-z
Radiophysics and Quantum Electronics, Vol. 63, No. 7, December, 2020
(Russian Original Vol. 63, No. 7, July, 2020)

SUPERCONDUCTING RECEIVERS FOR SPACE, BALLOON, AND GROUND-BASED SUB-TERAHERTZ RADIO TELESCOPES

Yu. Yu. Balega,[1] **A. M. Baryshev,**[2] **G. M. Bubnov,**[3,4]
V. F. Vdovin,[3,4,5] **S. N. Vdovichev,**[4]
A. A. Gunbina,[3,4,6*] **P. N. Dmitriev,**[6 †]
V. K. Dubrovich,[7] **I. I. Zinchenko,**[3,8]
V. P. Koshelets,[5,6] **S. A. Lemzyakov,**[9,10]
D. V. Nagirnaya,[6] **K. I. Rudakov,**[2,6] **A. V. Smirnov,**[5]
M. A. Tarasov,[6] **L. V. Filippenko,**[6] **V. B. Haikin,**[7,11]
A. V. Khudchenko,[5,6] **A. M. Chekushkin,**[6]
V. S. Edelman,[9] **R. A. Yusupov,**[6] **and G. V. Yakopov** [1]

UDC 520.8.056

We give a review of both our own original scientific results of the development of superconducting receivers for sub-terahertz astronomy and the main leading concepts of the global instrumentation. The analysis of current astronomical problems, the results of microwave astroclimate research, and the development of equipment for sub-terahertz radio astronomy studies justify the need and feasibility of a major infrastructure project in Russia to create a sub-terahertz telescope, as well as to enhance the implementation of the ongoing Millimetron and Suffa projects. The following results are discussed: i) superconducting coherent receivers and broadband sub-terahertz detectors for space, balloon, and ground-based radio telescopes have been developed and tested; ii) ultrasensitive receiving systems based on tunnel structures such as superconductor — insulator — superconductor (SIS) and superconductor — insulator — normal metal — insulator — superconductor (SINIS) have been created, fabricated, and examined; iii) a receiving array based on SINIS detectors and microwave readout system for such structures has been implemented; iv) methods for manufacturing high-quality tunnel structures $Nb/AlO_x/Nb$ and $Nb/AlN/NbN$ based on niobium films with a current density of up to 30 $\mathrm{kA/cm^2}$ *have been developed. Receivers operated at 200 to 950 GHz and having a noise temperature only a factor of 2 to 5 higher than the quantum limit have been created and tested.*

* aleksandragunbina@mail.ru
† Deceased

[1] Special Astrophysical Observatory of the Russian Academy of Sciences, Nizhny Arkhyz, Russia; [2] Astronomical Institute of the Groningen University, Groningen, the Netherlands; [3] Institute of Applied Physics of the Russian Acedemy of Sciences, Nizhny Novgorod; [4] R. E. Alekseev State Technical University of Nizhny Novgorod, Nizhny Novgorod; [5] Astrospace Center of the P. N. Lebedev Physical Institute of the Russian Academy of Sciences, Moscow; [6] V. A. Kotelnikov Institute of Radio Engineering and Electronics of the Russian Academy of Sciences, Moscow; [7] St. Petersburg Branch of the Special Astrophysical Observatory of the Russian Academy of Sciences, St. Petersburg; [8] N. I. Lobachevsky State University of Nizhny Novgorod, Nizhny Novgorod; [9] P. L. Kapitsa Institute of Physical Problems of the Russian Academy of Sciences, Moscow; [10] Physical and Technical Institute of Moscow, Moscow; [11] Peter the Great State Polytechnical University of St. Petersburg, St. Petersburg, Russia.
Translated from Izvestiya Vysshikh Uchebnykh Zavedenii, Radiofizika, Vol. 63, Nos. 7, pp. 533–556, July 2020. Original article submitted June 9, 2020; accepted July 31, 2020.

1. INTRODUCTION

Millimeter- and submillimeter-wave astronomy currently determines the frontier of astrophysical research in many ways. The obtaining of an image of the "shadow" of the supermassive black hole in the M87 galaxy is one of the most prominent recent achievements [1]. Due to combining millimeter-wave radio telescopes into a unified network called the "Event Horizon Telescope," this work has been done by joint efforts of observatories in a number of countries around the world [2]. A large number of new important results were obtained in areas such as exploration of the early Universe and distant galaxies, the study of the formation of stars and planets, the analysis of objects in the Solar system, etc.

All 75 years of development of the Faculty of Radiophysics at the Lobachevsky State University of Nizhny Novgorod, radio astronomy and the development of equipment for radio-astronomy research have been key and, undoubtedly, successful areas of activity of its team. This work was done at the highest international level and on the basis of extensive Russian and international collaboration [3-12]. Following global trends, the studies started in the decimeter and centimeter wavelength ranges, advanced into the millimeter and sub-millimeter ranges. In recent years, research and development in the frequency range from 100 to 1000 GHz not only provide extensive material for astrophysicists, but also dictate new challenges to the developers of equipment in this range.

The significant atmospheric absorption of the waves of the considered range makes it necessary to study in detail the conditions of their propagation in the locations of telescopes and to place observatories in the highlands, on airplanes, balloons, and even on spacecraft [13–17].

The paper presents astrophysical motivation for the sub-terahertz astronomy development and a review on some of the original results of designing the necessary equipment by its authors. Back in the 1960s A. G. Kislyakov showed that only deep cryogenic cooling of instruments would provide the sensitivity levels required for solving astronomical problems. In the same years, foundations for superconducting receiving equipment were laid at the Kotelnikov Institute of Radio Engineering and Electronics of the USSR Academy of Sciences, which were later developed in close cooperation with representatives from the Nizhny Novgorod school of radiophysics [19–21].

At present, the development of ultrasensitive sub-terahertz receivers is one of the most successful fields in superconductor electronics. Both coherent receivers with mixers based on superconductor — insulator — superconductor (SIS) tunnel junctions and incoherent broadband detectors based on different effects in superconducting thin-film structures are intensely used. SIS mixers are the best input devices for coherent receivers at frequencies of 0.1 to 1.2 THz, and their noise temperature is limited only by quantum effects. The operation of SIS mixers in quantum mode was theoretically analyzed in the seminal paper [22], in which all the basic relations for the mixer were derived on the basis of the photon-induced quasiparticle tunneling effect and the possibility of mixer operation with amplification was predicted. In [23], the method of determining the noise temperature of a SIS mixer in quantum mode with allowance for the Heisenberg uncertainty principle is substantiated, and it is shown that the noise temperature of a SIS mixer in a two-band regime is theoretically limited only by the quantum value $hf/(2k_{\mathrm{B}})$ (here, h is the Planck constant, f is the frequency of the received radiation, and k_{B} is the Boltzmann constant). That is exactly why the heterodyne SIS receivers are used in the majority of both ground-based and spaceborne radio telescopes [24–32].

Exceptionally sensitive mixers of the range in the vicinity of 250 GHz were developed already at the end of the last century (their noise temperature was 10–15 K) [25, 33]. However, mechanical adjustment of the waveguide circuit breaker was required to obtain extremely low noise temperatures, which limited their wide application. Later, SIS mixers providing low noise temperatures in a wide input band without mechanical settings were created. High-frequency receivers of the largest multi-element radio astronomy interferometer of our time — Atacama Large Millimeter/submillimeter Array (ALMA) [28–31, 34, 35], which includes 10 frequency bands ranging from 35 to 950 GHz, could be taken as the example. All high-frequency bands are equipped with SIS mixers, namely, B3 (84–116 GHz), B4 (125–163 GHz), B5 (163–211 GHz), B6 (211–275 GHz), B7 (275–373 GHz), B8 (385–500 GHz), B9 (602–720 GHz), and B10 (787–950 GHz). The

noise temperature of the sideband-separating B6 receiver is 40–60 K (in a single-band regime; intermediate-frequency band 4–12 GHz) [28]. The two-band noise temperature of the B9 receiver increases from 60 to 120 K when the local-oscillator frequency is varied from 610 to 710 GHz in the intermediate-frequency band 4–12 GHz) [29].

Note that the Heterodyne Instrument for the Far Infrared receiver in the Herschel Space Observatory [32] included five SIS receivers of the bands 480–640, 640–800, 800–960, 960–1120, and 1120–1250 GHz; the two-band noise temperature of the receivers ranged from 50 to 1000 K, respectively. The SIS receivers will be actively used in the Millimetron project of Roskosmos [37] to conduct studies on astronomical objects with both ultra-high sensitivity in the single telescope regime and with an unprecedented high angular resolution in the ground–space interferometer regime.

The intense development of SIS receivers continues to date, its key directions are related to the creation of matrix receivers [37, 38] and extension of the reception range almost to an octave [39], as well as extension of the intermediate band of the receiver [40] and provision of the band separation regime at high frequencies [41, 42].

As a broadband direct detector, the authors study sensitive elements based on superconductor — insulator — normal metal — insulator — superconductor structures. In a broad sense, the term "SINIS structures" includes many devices [43–45] ranging from thermometers [46–48] and electronic coolers [49–52] to various detectors, such as the Andreev bolometer [53–55], a cold-electron bolometer [56–57], SINIS bolometers [58, 59], SINIS detectors [60, 61], and SINIS detectors with a suspended absorber and a high quantum efficiency [62, 63].

The idea of the Andreev receiver was intensely developed in the 1990s and was one of the most promising concepts for astronomical research at that time. However, it was shown in [55] that the DC measured noise-equivalent power is $5 \cdot 10^{-18}$ W/GHz$^{1/2}$ and deteriorates significantly (up to 10^{-14} W/GHz$^{1/2}$) during irradiation by a 300 GHz signal and the volt–watt sensitivity drops to 10^6 V/W. This impairment of the main characteristics of the receiver when exposed to an external signal is explained by the fact that at a frequency higher than the energy gap of the superconductor (i. e., more than 70 GHz for aluminum) the superconductor — normal-metal contacts become "transparent" to radiation. As a result, the Andreev contacts were replaced with capacitive ones (superconductor — insulator — normal metal), and a SINIS detector appeared. Currently, there is a prospect for the further development of the Andreev detector by replacing aluminum banks with banks made of niobium nitride, which will extend the range of such a detector to 1 THz.

The ideology of detectors based on SINIS structures was actively developed over the next 20 years: in [60, 61], different operating regimes of such detectors were demonstrated, and, in contrast to [56], the evaluation of the characteristics is based not on the heat balance equation, which does not take into account the quantum nature of absorption, but on the kinetic equation and collision integrals. In [64], it was experimentally confirmed that the electron cooling effect does not give the expected increase in the detector sensitivity. Different design features of such structures were studied [65], and it was found that large-volume superconductor electrodes should be formed to dilute hot quasiparticles for normal operation in order to avoid superconductor overheating. High quantum efficiency (15 electrons per 350 GHz radiation quantum) can be achieved by creating a "suspended" (detached from the substrate) absorber [63]. The following features have been achieved to date: wide dynamic range (30 dB), which is necessary to work under high background load (tens of picowatts), volt–watt sensitivity up to 10^9 V/W, and noise-equivalent power no more than 10^{-16} W/GHz$^{1/2}$, which can be reduced by improving the readout system. Such characteristics meet the requirements for use on ground-based high-altitude and balloon telescopes, but the practical exploitation of SINIS detectors at observatories has not yet been presented. As part of the work conducted by the authors of this paper, it is planned to introduce SINIS detectors for research at the LAT observatory for the first time [66, 67].

2. TOPICAL PROBLEMS OF SUB-TERAHERTZ ASTRONOMY. OBSERVATION AND EQUIPMENT PROBLEMS

For today, sub-terahertz astronomy has one of the most extensive lists of scientific problems which include observations of different astronomical objects in combination with the development of theoretical models. These models are necessary both for the planning of experiments and for the interpretation of their results (see, e. g., [68, 69]). Many of them are related to the study of the so-called cold Universe. Mostly these are dense interstellar gas–dust clouds, both in our Galaxy and in distant objects. They are interesting primarily because they undergo a star formation process, many aspects of which are still not fully understood. The sub-terahertz range is densely populated with spectral lines, which are mainly responsible for transitions between the rotational levels of molecules with a relatively low excitation energy. Along with the study of the cold Universe, sub-terahertz astronomy also gives a great contribution to the study of objects characterized by an extremely high energy release, such as the active cores of galaxies, which, apparently, are accreting supermassive black holes. It is possible to achieve the required ultra-high angular resolution, as well as to reduce the wave scattering effects along the line of sight exactly in this range. High hopes are pinned on the Millimetron project [69].

The question on the formation of the first stars and galaxies is very important for astrophysics. Here, there is a problem of studying the "dark ages" of the Universe, namely, the time interval between the epoch of recombination and the birth of the first stars. So far, there is no observational information about this period. It seems that the only way to obtain such information is to search for distortions of the Cosmic Microwave Background (CMB) spectrum created by simple molecules, which, according to the available models, should already be present in the Universe at this time [70]. However, the expected distortions are extremely small. One of the most promising molecules is the HeH^+ ion [71–73], which has only recently been reliably detected in space [74]. The search for the $J = 1 - 0$ line of the HeH^+ ion in the spectrum of a distant quasar with a redshift $z = 6.42$ identified a detail in the spectrum with a signal-to-noise ratio of about 3 [75], which does not allow talking about its reliable detection.

The background spectrum can also be distorted for other reasons, namely, due to the scattering of photons by a hot plasma and due to energy release in the pre-recombination epoch [76]. These distortions are also extremely weak.

Search for the manifestations of primary gravity waves that occur in inflation models at the first moments of life of the Universe is one of the most important problems in its research. As it now appears, the B mode of polarization of the microwave background is the only observational manifestation of these waves [77]. In addition to the primary gravity waves, the B mode can occur due to gravitational lensing and scattering by dust in the Galaxy. This component has been measured in a number of experiments [78]. However, the problem of seeking radiation with such polarization caused by primary gravity waves remains one of the most important.

The study of the early Universe requires refined methods and proceeds in several directions. The method of statistical description of the power spectrum of primary temperature fluctuations of the cosmic microwave background is one of the most developed methods at present time. In addition, the method of studying the global characteristics of the CMB frequency spectrum, which carry information about the global energy release in the epoch $z < 100000$, is used. Spectral distortions in the region of sub-terahertz waves are the main source of information. Information about the parameters of the early Universe can also be obtained by studying the spatial distribution of galaxies.

Despite the modern achievements in the development of instruments for sub-terahertz astronomy, some areas of research remain completely uninvolved in the experiment. In particular, we are talking about the search and study of the primary small-scale spectral–spatial fluctuations of the CMB intensity, which are formed in the epoch of recombination of primary helium and hydrogen at redshifts of about 6000–1000. According to the results of the latest studies of the Planck mission [79], there is a map of the CMB brightness distribution in the form of spots with different amplitudes and spatial scales to date. They are located in a certain range of distances from us. By its appearance and physical grounds, this range can be considered

as some "third" sky, which follows after the "first" sky (the Earth's atmosphere) and the second "sky" (the region of the stars and galaxies).

Relatively high-resolution spectroscopy combined with the study of individual fluctuations, that is, the search and study of spectral–spatial fluctuations in the CMB temperature is the most obvious and promising approach for the study of the frequency spectrum of individual spots on this map. There is already a fairly large input [80–84] on different aspects of physical processes and their quantitative calculation in the field of the theory of such fluctuations. In particular, the picture of the spatial and spectral distribution within a separate protoobject is described in considerable detail [80–84]. The distribution of brightness (intensity) over the fluctuation radius for sufficiently small initial sizes of protoobjects has an almost universal form due to the fact that it is formed at the stage of the last scattering in the epoch of hydrogen recombination [85, 86]. The radiation of the protoobject is locked up near it up to this moment because of the large optical depth of the Thomson scattering by electrons.

The summation of these fluctuations along the line of sight in blending is another important feature. The summation result will be averaged in the case of a continuum Planck spectrum of each individual fluctuation due to the same dependence of the photon frequency and temperature on the redshift z. Each fluctuation lying on the line of sight has its own system of spectral details corresponding to the z value of this fluctuation. Such components will not be imposed on each other when summing them up. Thus, a complete three-dimensional picture of the distribution of protoobjects can be obtained. A more detailed view of the spectrum of a single fluctuation is determined by the interaction of radiation with hydrogen and helium atoms in the resonance lines of the Lyman series and luminescence. The first mechanism produces an effect in the Wien region of the CMB and has the form of characteristic jumps [80, 81]. The second mechanism gives distortions in the Rayleigh–Jeans [82–84] wing of the CMB. The spectral bands are determined by the size of the initial fluctuation and will be of the order of a few percent of the center frequency. The distortion amplitude is determined by the initial intensity of the fluctuation and the quantum efficiency of the spectrum redistribution.

Solving these problems requires the development and manufacture of spectral heterodyne, filter, and bolometer receivers designed to operate in atmospheric transparency windows in ground-based instruments, and for space and balloon instruments without these restrictions. In particular, it is desirable to have a satellite similar to those being prepared as a part of the Millimetron [17, 36], JWST [87], and other missions for the problems of studying the early Universe. However, a low-Earth orbiting satellite (500 to 1000 km altitudes) with a relatively small telescope (1.5 m in diameter) having a spatial resolution of 4–5 min of arc per pixel of the matrix and a receiving matrix in a range of 0.5 to 1.2 THz can also be applied. The matrix receiver should have a spectral resolution of 5–10 GHz and the maximum possible sensitivity. In principle, such an experiment can be performed using a ground-based receiving system similar to the one described above. In this case, it should be located at the highest possible altitude in the mountains with a good astroclimate (Tibet, Himalayas, Pamir, Yakutia, etc.).

Going into space and onboard other aircraft, such as balloons, airplanes, spaceships, etc. is predetermined for the sub-terahertz range by the high atmospheric absorption of these waves, to which many studies and publications are dedicated. However, the issue of its study, referred to as the study of astroclimate [88] in the sub-terahertz range in the professional environment, as well as the development of specialized equipment and the improvement of methods are very topical at present. These studies were also initiated by A. G. Kislyakov and co-authors. The latest results obtained by the authors of this review are summarized below. They showed that the integral transparency of the atmosphere (the so-called optical depth) caused by the absorption of waves in this range in water vapor and oxygen [89] is the main factor of astroclimate in the sub-terahertz range. This distinguishes the concepts of microwave and optical astroclimate to some extent; in the latter, the role of oxygen is insignificant.

The choice of the frequency range in the studies is determined by the operating range of the observatory and is linked to the transparency windows, i. e., local minima of the absorption spectrum at which the observatory is assumed to operate or already operates. MIAP-2 (a two-channel microwave atmospheric ab-

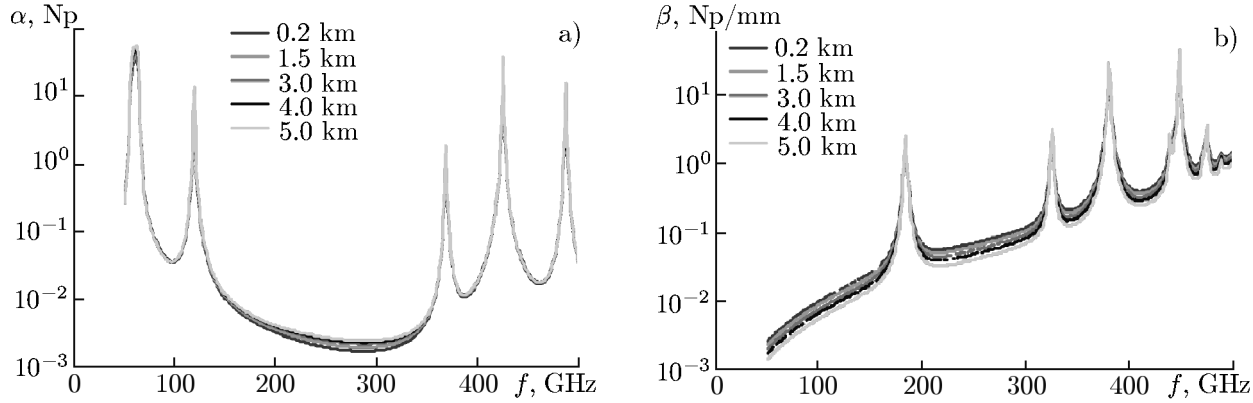

Fig. 1. Spectral characteristics of the specific absorption coefficients in the sub-terahertz range from different altitudes: (*a*) the spectrum of a dry absorption coefficient reduced to the sea level (α); (*b*) the spectrum of a specific absorption coefficient in water vapor (β).

sorption meter) was developed at the IAP RAS and CJSC GYCOM, a scientific and production enterprise, on request of the R. E. Alekseev State Technical University of Nizhny Novgorod. This device measures the optical depths by the method of atmospheric cuts in transparency windows in the 2- and 3-mm wavelength ranges in automatic mode [90]. The technique and equipment are continuously upgraded [91, 92]. Eleven expeditions have been held since 2012 to examine the statistics of integral transparency of more than 20 sites at which a sub-terahertz radio telescope can be constructed [93].

From an astroclimate point of view, the dissipation of sub-terahertz waves consists of absorption in water vapor and "dry" absorption, as well as scattering and absorption in clouds and fog [90, Eq. (2)]. Dry absorption is linked to the altitude of the area and varies slightly with temperature, while absorption in water vapor is highly dependent on meteorological conditions and the local climate of the area, so it is subject to diurnal and seasonal variations. The integral moisture content (Precipitable Water Vapor, PWV), which determines the main variable component, is the most universal astroclimate characteristic. Knowing the PWV and the coefficients of the PWV conversion into optical depth, it is possible to estimate the atmospheric transparency at any frequency of the sub-terahertz range using proven absorption models, e. g., MPM Liebe [94], HITRAN [94], or GEISA [96].

The spectra of a dry absorption coefficient reduced to the sea level (α) and a specific absorption coefficient in water vapor (β) are shown in Fig. 1. A typical winter profile of the atmosphere on flat terrain based on weather sounding data is used as the example to calculate the spectrum in terms of the MPM Liebe model. Variations in the absorption coefficients are particularly well seen in the transparency windows. Both coefficients were found to decrease with altitude in winter conditions with a small PWV (3–5 mm). The coefficient α increases and β decreases with altitude in wet summer conditions (PWV$>$ 15 mm). The more accurate the information about these coefficients, the more accurately the optical depth can be calculated in the desired frequency ranges using PWV. In this regard, there is a need for detailed and direct research on the sites of the proposed construction of new sub-terahertz telescopes, as well as for the further development of equipment and techniques, especially for adding a direct meter of atmospheric absorption in transparency windows in the vicinity of 1.3 and 0.87 mm to the existing equipment.

3. LOW-NOISE 211–275 GHz BAND SIS MIXER FOR RADIO ASTRONOMY

The team of authors has been successfully developing superconducting receivers of the millimeter wavelength range since the 1980s and has gained the first experience of successful operation of its SIS receiver at a frequency of 0.1 THz at the RT-25 $\times$ 2 radio telescope in Zimenki. These works were initiated by A. G. Kislyakov [97]. Successful cooperation with the Nizhny Novgorod school of radiophysics did not stop in subsequent years. Now it is aimed at developing equipment for the Suffa telescope under construction [72].

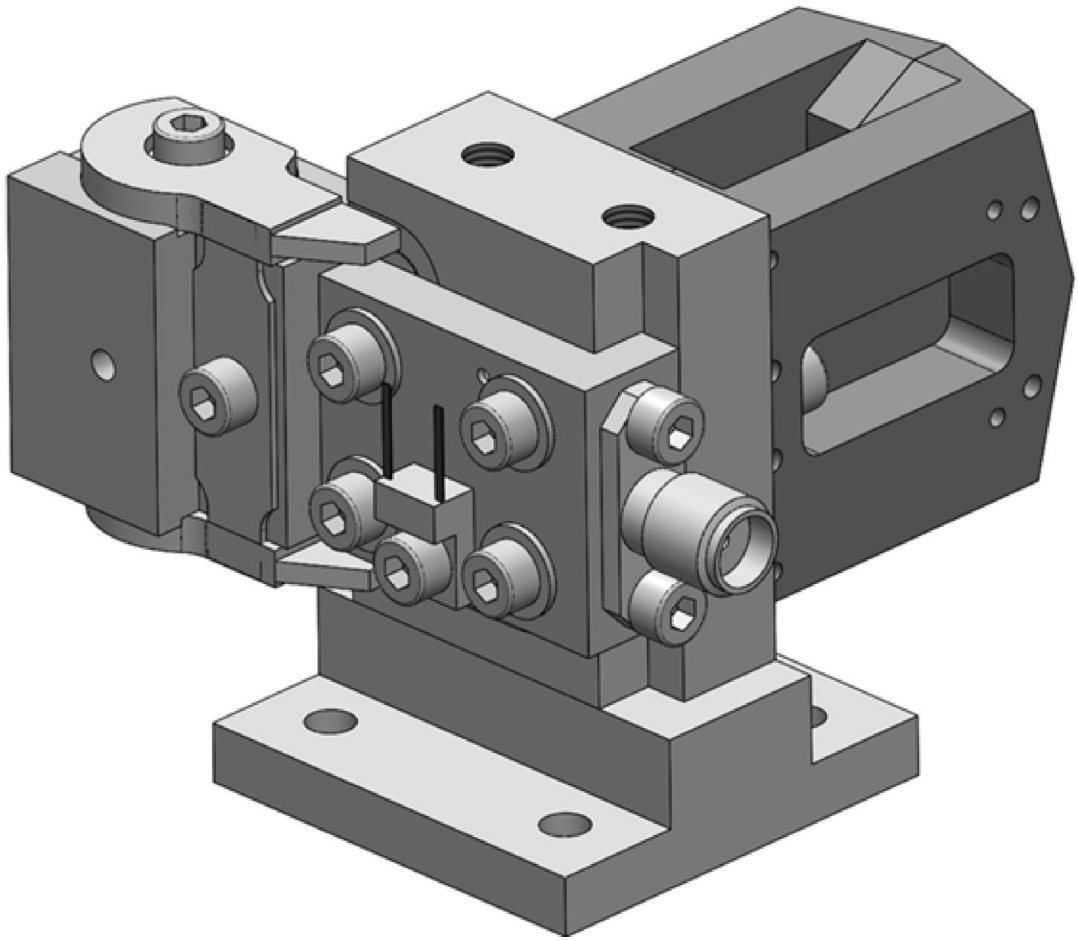

Fig. 2. A three-dimensional model of the 211–275 GHz mixing unit (a plug-in board of the mixer unit with a SIS transition is seen in the foreground and the output of an intermediate frequency signal is shown on the right).

Mixers with a noise temperature of less than 50 K in the frequency range of 211–275 GHz are required for the successful fulfillment of the already started radio astronomy projects, such as Suffa and the Roskosmos Millimetron program. To solve this problem, the topology of the mixing element was developed, its characteristics were simulated and optimized, and experimental $Nb/AlO_x/Nb$ structures (having an area of $1\mu m^2$) with low leakage currents (the ratio of resistances above and below the energy gap was more than 30 at liquid helium temperature, which is close to the maximum possible value and is required to obtain extremely low noise temperatures) were manufactured. It is also necessary to compensate for the significant capacitance of the SIS junction ($C \approx 0.085$ pFμm^2) in order to achieve a low noise temperature. As a result, the impedance of the structure is reduced to a few ohms, and it is necessary to coordinate the final impedance of the SIS junction at a high frequency with the impedance of the waveguide (about 400 Ω), which was done by using a planar structure consisting of segments of coplanar and microstrip lines of $Nb/SiO_2/Nb$ [99]. The receiving element was made on a quartz substrate with a thickness of 125 μm. Blocking filters were used in the design of the mixing element to prevent high-frequency signal leakage [99]. The receiving element was perpendicular to the plane of wave propagation in a rectangular waveguide with a 500×1000 μm cross section and was located at a distance of 230 μm from the closer at the end of the waveguide. The mixing waveguide unit consisted of a central part with a waveguide, a closer unit, a magnetic field setting unit, and an input horn (see Fig. 2).

The I–V curve of the $Nb/AlO_x/Nb$ mixing element with an area of 1 μm^2, which was measured in the voltage setting regime, is shown in Fig. 3*a* by a dash–dotted line; the critical current of the SIS junction

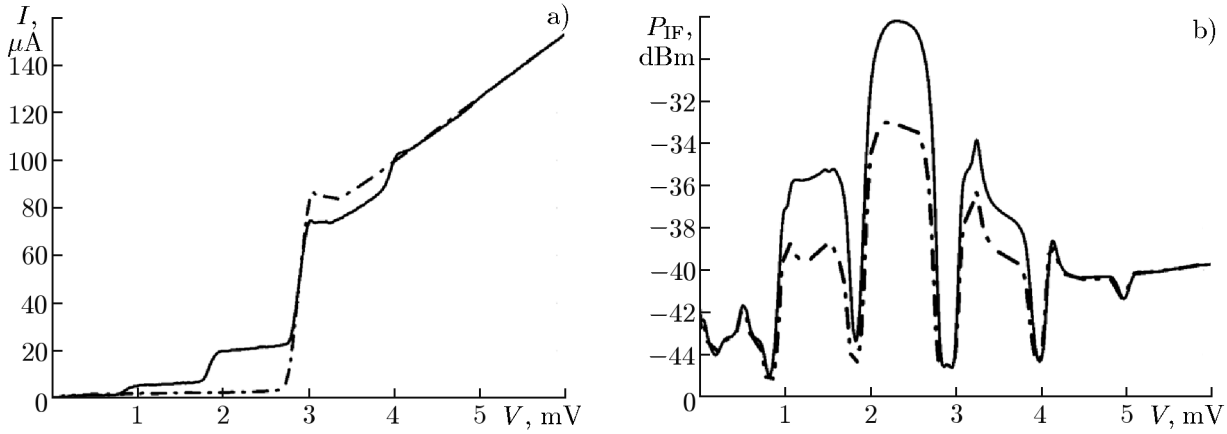

Fig. 3. Experimental characteristics of the SIS mixer: (*a*) the I–V curve of the mixing element. The dash–dotted curve shows an autonomous characteristic and the solid line, when affected by the local oscillator at a frequency of 240 GHz with optimal power. (*b*) The dependences of the output signal power P_{IF} of the SIS receiver on the bias voltage, measured for the local-oscillator frequency 240 GHz at an intermediate frequency of 6.5 GHz with cold (78 K) and warm (295 K) input loads (dashed and solid lines, respectively).

is suppressed by the magnetic field. The I–V curve affected by a local oscillator with a frequency of 240 GHz and an optimal power for the SIS mixer operation is shown by a solid line. The quasiparticle jumps of the current, whose voltage size is determined by the frequency of the local oscillator, are clearly seen [100, 22]. The noise temperature of the mixer in the two-band regime was determined by the standard method of measuring the Y-factor; an absorber at 295 K was used as a "hot" load, and an absorber cooled to 78 K with liquid nitrogen was used as a "cold" load. Figure 3*b* shows the dependence of the output signal power of the SIS receiver on the bias voltage for two loads measured at a local-oscillator frequency of 240 GHz. Since the responses in Fig. 3*b* are presented in decibels, the value of the Y-factor can be determined by subtracting these two dependences. It can be seen that the Y-factor reaches 5 dB at the best points, which corresponds to a receiver noise temperature of 24 K. The dependence of the two-band noise temperature of the SIS receiver on the local-oscillator frequency was measured in [73]. The noise temperature values were obtained without correction for losses in the beam splitter and the cryostat input window; they were only twice as high as hf/k_B in the range from 240 to 265 GHz and meet the technical requirements for a receiver in the range 211–275 GHz for the receiving system of the Millimetron space radio telescope.

4. INTEGRATED SUPERCONDUCTING 450–650 GHz BAND RECEIVER

Local oscillator is one of the most important elements in coherent signal reception; its tuning range, spectral characteristics, and the range of matching with the mixer affect the characteristics of the device as a whole. The concept of a superconducting integrated receiver [101, 102], which is based on a fundamentally new approach, namely, integration of a superconducting heterodyne oscillator with a quantum mixer due to the quasiparticle nonlinearity of tunnel junctions and a superconducting antenna in a single chip, was proposed and tested at the Kotelnikov Institute of Radio Engineering and Electronics of the Russian Academy of Sciences. The chip is manufactured on a silicon substrate with a thickness of 0.5 mm using modern microelectronics methods and contains a superconducting mixer, an immersion lens dipole or slot antenna, a superconducting local oscillator, and an additional mixer for the phase-locked heterodyne frequency system. The size of the circuit with contact pads is 4×4 mm. Superconducting integrated heterodyne oscillators based on distributed Josephson junctions provide a unique combination of mass-dimensional and frequency characteristics and still have no analogues.

Figure 4 shows a photograph of the center of the receiver chip with a double-slot antenna designed to study the Earth's atmosphere from a high-altitude balloon (international project TELIS) [103–107]. Radia-

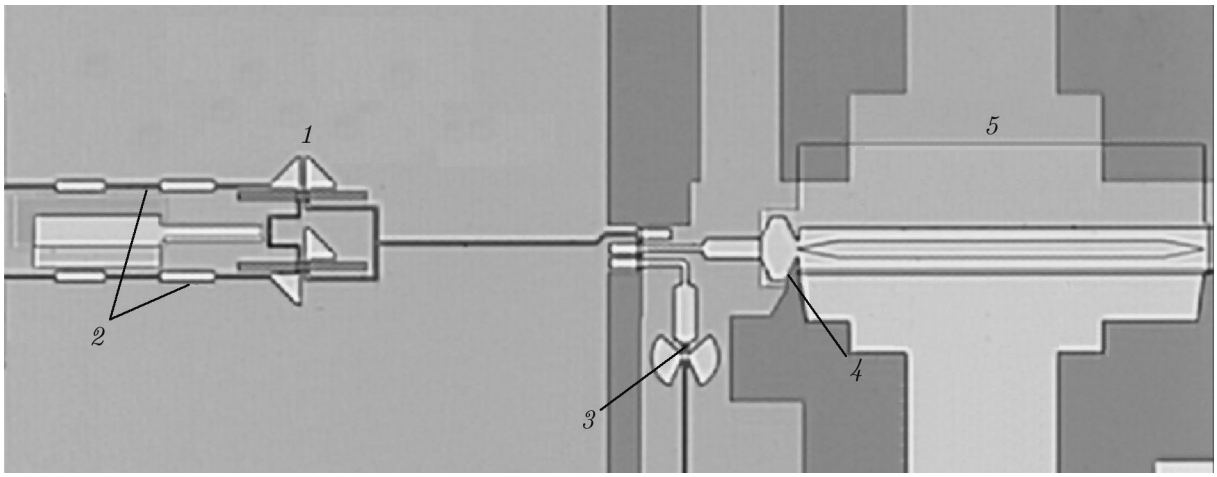

Fig. 4. A photograph of the center of the integrated receiver chip with a double-slot antenna (an 1.2×0.5 mm region is shown): *1* is a double-slot antenna with a SIS mixer (transition area $0.8\ \mu\text{m}^2$), *2* is a rejector filter of the intermediate frequency, *3* is a harmonic SIS mixer with an area of $1\ \mu\text{m}^2$, *4* is an impedance transformer, and *5* is a local oscillator (transition size $400 \times 16\ \mu$m).

tion from a superconducting heterodyne oscillator is transmitted through a matching circuit (an impedance transformer) to a microstrip line with an impedance of about 20 Ω and then distributed between two SIS mixers using a power divider (which also isolates the mixers and the oscillator with respect to the direct bias current). The spectral characteristic of a superconducting heterodyne oscillator has a Lorentz shape, the typical half-width of which ranges from hundreds of kilohertz to tens of megahertz, depending on its design and the choice of the operating point. The use of oscillators with a wide autonomous line as a heterodyne in receivers with a high spectral resolution requires a wideband automatic frequency control system of the heterodyne. A harmonic SIS mixer is added to the receiver circuit to generate the intermediate frequency signal of the phase-locked loop (400 MHz). The band of this system is about 15 MHz, which provides a spectral quality (ratio between the power in the spectral peak of this phase-locked frequency oscillator and its total power) above 50% with an up to 5-MHz wide autonomous line of the superconducting heterodyne oscillator. Figure 5 shows the spectral characteristics of a stabilized superconducting heterodyne oscillator measured relative to the reference synthesizer.

There were four successful launches of the TELIS spectrometer onboard a high-altitude balloon together with the MIPAS-B spectrometer. The instrument demonstrated the ability to work under extreme conditions (a temperature of $-90\,^\circ$C) and allowed us to collect a large amount of scientific information confirming the high spectral resolution and sensitivity of the device. Several hundred limb scans were recorded; the spectra of the gas components of the Earth's atmosphere were detected. The spectra of compounds of chlorine, bromine and other impurities responsible for the destruction of the ozone layer in the Earth's atmosphere were obtained during the flight on a high-altitude balloon; the diurnal variations of different components of the atmosphere were measured during the flight. The diurnal cycles of the concentration of chlorine monoxide formed during the catalytic decomposition of ozone under the influence of chlorofluorocarbons have been studied. The isotope spectra of different substances, including water and hydrochloric acid HCl, were also obtained in the altitude range 12–36 km (see Fig. 6) [105–107]. The concentrations of the observed gases were estimated as 0.5 and 1.5 parts per billion by volume (ppbv) for the $H^{37}Cl$ and $H^{35}Cl$ lines, respectively. BrO spectra were recorded in the terahertz range for the first time, the signal intensity in this case was only 0.3 K [105–107], which corresponds to an extremely low concentration of several parts per trillion by volume (pptv). The integrated spectrometer created on the basis of the flight instrument was successfully used in the laboratory for gas spectroscopy and for studying radiation from newly created superconducting oscillators in the sub-terahertz range [108, 109].

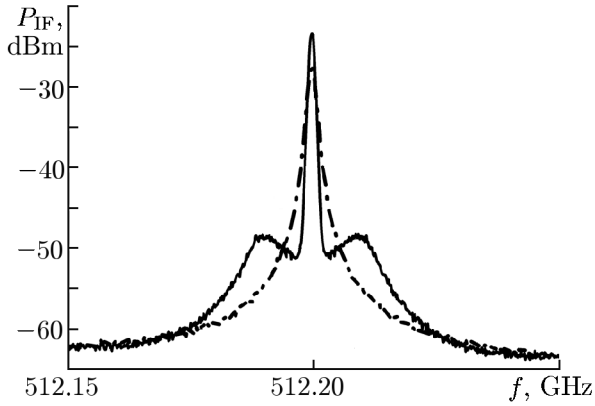

Fig. 5. Spectral characteristics (intermediate-frequency signal power P_{IF}) of a superconducting heterodyne oscillator measured at a frequency of 512.2 GHz relative to the reference synthesizer (100 MHz band, spectrum analyzer resolution 1 MHz). The radiation spectrum measured in the frequency stabilization regime (the autonomous line is 1.5 MHz wide) is shown by a dash–dotted line; the spectrum measured in the phase-locked frequency regime (spectral quality 93.5%) is shown by a solid line.

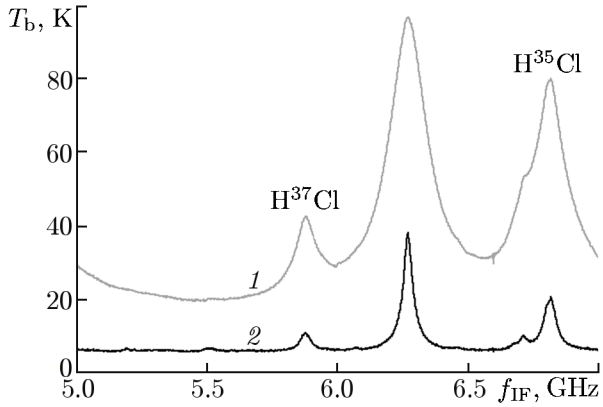

Fig. 6. Spectra of two isotopes of HCl and ozone (T_b is the brightness temperature and f_{IF} is the intermediate frequency) measured using a superconducting integrated receiver from a high-altitude balloon (TELIS project); the heterodyne frequency is 619.1 GHz. The instrument was located at an altitude of 38 km, the measurements were made in two directions of the telescope axis, namely, tangent at an altitude of 25 km (curve *1*) and elevated by 6° relative to the horizon (*2*).

5. SIS MIXER FOR THE 800–950 GHz BAND

Atmospheric absorption strongly increases with increasing frequency in the sub-terahertz range, which is due mainly to the presence of water vapor. Even in such a unique place as the Chahnantor plateau in Chile, located in the desert at an altitude of 5 km, where the advanced terahertz radio telescopes ALMA [110] and APEX [86] are installed, atmospheric transparency in the zenith at frequencies of 800–950 GHz rarely exceeds 0.6, even at the best time of the day. Because of this, the signal-to-noise ratio when astronomical objects are observed is strongly affected by atmospheric noise. The use of sideband-separating receivers reduces the contribution of atmospheric noise by half compared to two-band receivers. Reducing the noise of warm optics and the atmosphere by half was exactly the key argument for installing sideband-separating receivers at frequencies of up to 500 GHz on the ALMA interferometer. Two-band receivers are still used for higher-frequency bands because the technology was not sufficiently developed to make sideband-separating receivers at the time of the interferometer design.

Within the framework of international cooperation with our participation, a waveguide sideband-separating SIS mixer for the 800–950 GHz [42] band was successfully demonstrated recently for the first time. Single-band noise temperature ranges from 450 to 900 K, and the band separation efficiency exceeds 15 dB for 95% of the range. The SIS mixers for this receiver were made on the basis of Nb/AlN/NbN tunnel junctions with a high current density of up to 30 kA/cm^2. To ensure low losses of the detected terahertz signal, the lower electrode of the supply microstrip line was formed from an NbTiN film having a high critical temperature of more than 14 K, and as a consequence an extremely low resistance, at frequencies of up to one terahertz. The layer was about 300 nm thick. A layer of SiO_2 insulator with a thickness of 250 nm was deposited on top of it, and an Al film with a thickness of about 500 nm, from which the upper electrode of the microstrip line was formed, was deposited from above. The tunnel SIS junction was placed on top of the lower electrode of the microstrip so that the Nb and NbTiN layers were in contact, while the upper layer of the NbN junction was in contact with the aluminum upper electrode. The key details of the manufacturing processes of the described structures, as well as the details of the electromagnetic design, are given in [31,

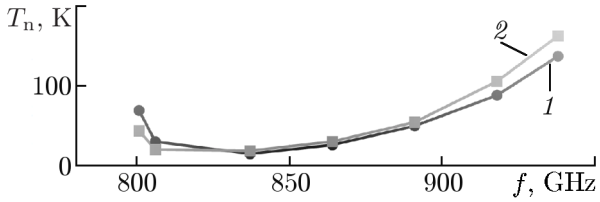

Fig. 7. Noise temperature T_n as a function of the reference oscillator frequency for two SIS mixers (marked with numbers *1* and *2*). The data is adjusted for the contribution of noise from the beam splitter, which is used for input of the reference oscillator signal and is kept at room temperature.

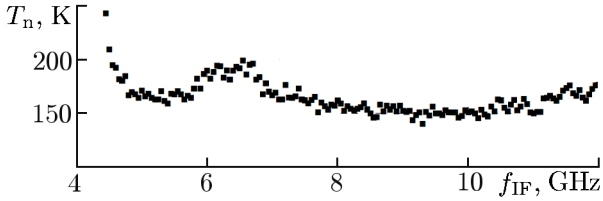

Fig. 8. Noise temperature as a function of the intermediate frequency for mixer *1* (see Fig. 7). The data is adjusted for the contribution of noise from the beam splitter. The measurement corresponds to a reference oscillator frequency of 837 GHz.

112]. The created SIS junctions have the following parameters: gap voltage $V_g = 3.1$ mV at a temperature of 4.2 K, area about $S = 0.5\ \mu m^2$ of a separate tunnel junction, normal-state resistance $R_n = 7\ \Omega$ of a double junction, quality $Q = 25$ of the tunnel junction determined by the subgap leakage current (the quality is calculated as the ratio between the subgap resistance R_j and the normal-state resistance R_n).

The so-called twin design [113], namely, a chip with two SIS junctions that are located close to each other at the end of the microstrip line, was chosen to ensure the broadband response of the receiver. A small change in the tuning structure, which shifts the optimal matching up the frequency by about 100 GHz, is a distinctive feature of the SIS mixers presented in this paper as compared with those described before in [31] and [112]. This improves significantly the matching of the mixer with the external signal at the upper frequencies of the required range and provides a more uniform noise temperature in the range 800–950 GHz.

Figure 7 shows the noise temperature measurements of two SIS mixers in a two-band regime. The corresponding frequency of the reference oscillator is plotted along the abscissa axis. Each point on the curve reflects the result of averaging over the intermediate frequency in the range 4–12 GHz. The noise temperature is measured by the standard Y-factor method described above, using an absorber with temperatures of 300 and 78 K. It should be noted that the diagram shows the noise temperature adjusted for the contribution of noise from the beam splitter, which is used for input of the reference oscillator signal and has a temperature of 300 K. This beam splitter is a mylar film with a thickness of 12 μm, which has a transparency varying from 0.89 at 800 GHz to 0.85 at 950 GHz. It can be seen from the above data that the noise temperature of the SIS mixers varies in a range of 210 to 350 K.

Figure 8 shows the noise temperature as a function of the intermediate frequency of the mixer, while the reference oscillator emits at a frequency of 837 GHz. The diagram shows that the noise temperature decreases to 200 K and is fairly evenly distributed in the given range. The peak at 4.2 GHz is an artifact and is related to the resonance in the intermediate-frequency amplifier. Further, this defect was eliminated when the characteristics of the sideband-separating receiver were measured [42].

6. INCOHERENT CRYOGENIC DETECTORS

In addition to the coherent receivers that provide high-efficiency astronomical spectral observations in the sub-terahertz range, as was noted in Sec. 2, ultrahigh-sensitivity observations without preserving phase information, or incoherent reception, are of great interest. At present, a kinetic inductance detector is one of its most promising concepts. Back in 1973, it was shown [114] that deep (below the liquid helium temperature) cryogenic cooling of such detectors built on a nonlinear superconducting inductance, rather than a nonlinear resistance and capacitance, and *a priori* having a certain finite and non-zero noise resistance, is able to provide the minimal noise of such a detector. The intense development of kinetic inductance detectors by different research teams started in the 2000s (see, e. g., [115–117]), and this idea has brilliantly been developed to date [118, 119] in world practice. A four-band sub-terahertz receiver built on detectors with kinetic inductances was successfully tested onboard the Olympo balloon observatory a short

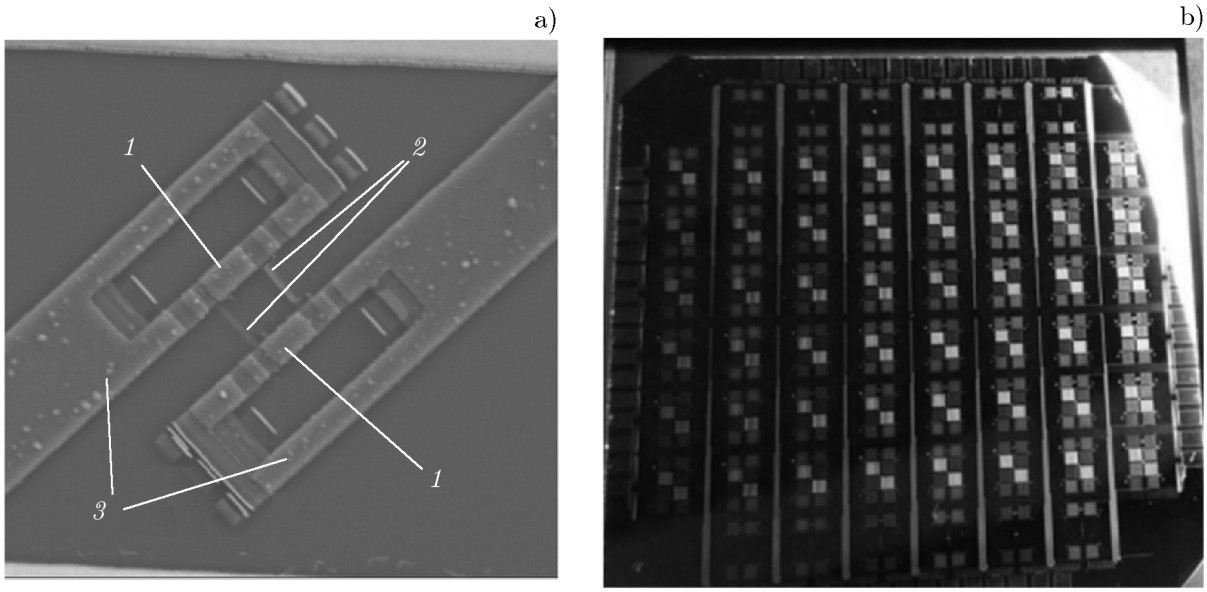

Fig. 9. The SINIS detector (*1* is normal metal — insulator — superconductor, *2* is the absorber, and *3* is the superconducting electrode *a*) and a multi-pixel structure based on such detectors (*b*).

time ago [120] with the participation of representatives from the Nizhny Novgorod school of radiophysics. A bolometer at the edge of a superconducting transition [121], the principle of operation of which is based on the abrupt transition of a superconducting film to a resistive state when irradiated with an external signal, is another promising type of direct receivers. Major projects, such as SCUBA-2 [122], BICEP2, Keck, and Spider CMB Polarimeters [123], or the upcoming LiteBIRD mission [124], can be taken as the examples of using such bolometers in observatories. There are many other competitive ideologies for constructing superconducting detectors of sub-terahertz waves, such as hot-electron bolometers [125] and detectors with a SINIS structure [126]. In particular, hot-electron sub-terahertz and terahertz bolometers created by the Russian team of the Moscow State Pedagogical University, have successfully been used in ground-based and spaceborne observatories [125]. The authors of this paper are intensely engaged in the development of the SINIS concept, and a sub-terahertz receiver for the LAT optical telescope is designed exactly on such a structure.

The SINIS detectors, which are also called bolometers in some regimes, represent a promising type of incoherent receivers in the sub-terahertz range. The development of such detectors proceeds in two directions. The first is to create antenna arrays for receiving incoming radiation with high power in one pixel. The second is the creation of multi-pixel receivers with high-frequency readout to ensure frequency channel separation (multiplexing) and reduce the thermal load of the cryostat and the contribution of noise of the readout system. A single SINIS detector and a general view of the multi-pixel structure based on the matrices of such detectors are shown in Fig. 9.

6.1. Matrix of electrically small antennas in the 200–400 GHz band

Antenna matrices where the power of the incoming radiation is distributed among the detectors are conventionally employed to extend the dynamic range and get a high power in one pixel. A matrix of planar half-wave antennas connected in series or in parallel (depending on the readout equipment) with a period of the order of the wavelength is the classical example [127-129]. A matrix of 10×10 antennas will occupy an area of about 100 squares of the wavelength. In this case, the bandwidth will be quite narrow and determined by the band of a single antenna. The use of arrays of electrically small antennas was a radical step to extend the reception band and reduce the occupied area [130, 131]. This design is close in

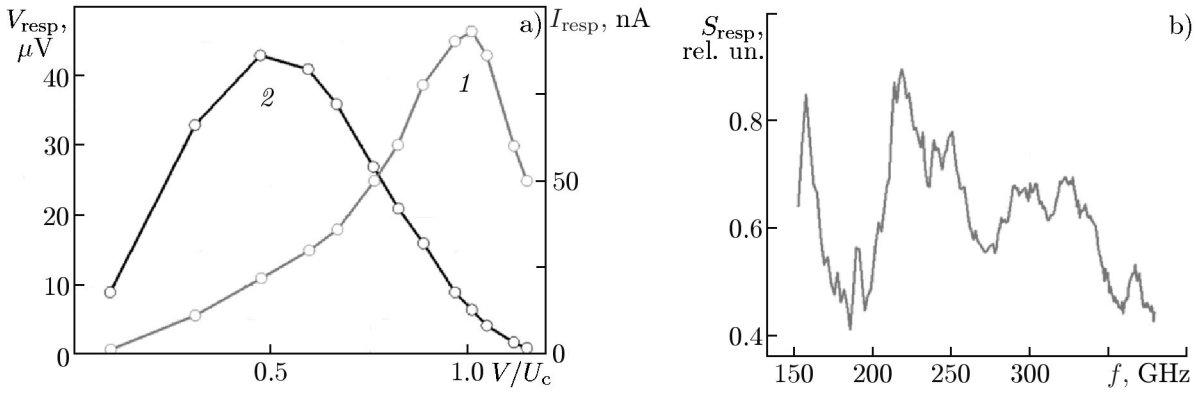

Fig. 10. Results of experimental measurements of the characteristics of the matrix of electrically small antennas: (*a*) is the current (1) and voltage (2) response for the matrix of parallel rings in the form of a metamaterial at a temperature of 100 mK and a radiation power of 3.7 pW (the reduced voltage is plotted along the horizontal axis); (*b*) spectral response.

its parameters to a distributed absorber. Samples with metamaterials for the 200–400 GHz band with an outer diameter of 56 μm of the ring antenna and a period of 70 μm were developed. The area of the matrix of 10×10 elements is 700×700 μm. Two detectors based on the SINIS structure are integrated into each planar antenna with a size less than 1/10 of the wavelength. Thus, 200 detectors are located on an area of 0.49 mm^2, i. e., the power per unit area for the matrix of metamaterials will be a factor of 46 higher than in the case of a matrix of half-wave rings with a diameter of 300 μm and a period of 475 μm with the same saturation power per detector. Herein, the pixels of the image matrix can be put much closer to each other, and a factor of 46 more pixels can be placed in the focal plane.

The voltage responses were $2.8 \cdot 10^9$ V/W for 30 fW and $3.5 \cdot 10^8$ V/W for 2 pW for the matrix of rings in the form of metamaterials connected in series (see Fig. 10*a*). A backward wave oscillator (BWO) was used as a source when the spectral response was measured. The BWO signal passing through the windows of the cryostat enters the test sample. The spectral response (see Fig. 10*b*) of the metamaterial turns out to be quite wide and more uniform compared to the matrix of standard ring antennas, and the observed spectral inhomogeneities correspond to losses and reflections in the quasi-optical path, which includes windows and filters at the three temperature stages of the cryostat. A detailed method for measuring the spectral response of different matrices based on SINIS detectors is presented in [132].

6.2. 90-GHz Band SINIS Bolometer with Microwave Readout

The currently used cryogenic detectors with readout systems on cooled and uncooled field-effect transistors with intrinsic noise at a level of 10 nV/Hz$^{1/2}$ have no prospects for application in modern multi-pixel receiving systems of radio-astronomical observatories. At present, receivers can contain up to half a million sensors, such as CMB Stage IV [133]. If separate amplifiers with a mass of 1 g per channel are installed for such an array of sensors, then the mass of the amplifier unit will be 500 kg, and a million wires will need to be attached to the cryostat. A significantly wider frequency range, a few gigahertz, is required for a large number of channels. Readout systems with frequency-separated channels have been created and are successfully used for microwave detectors based on kinetic inductance. An ultrahigh-frequency readout and multiplexing system described in [134], where 5000 pixels are simultaneously read at a temperature of 250 mK, can be taken as the example.

An integrated reception structure (see Fig. 11) [135], including a SINIS detector, a double-slot antenna at a signal frequency of 90 GHz, and a superconducting coplanar resonator connected through a coplanar coupler with coplanar readout line to the 2.0, 3.2, 4.2, and 6.0 GHz channels (see Fig. 12), has been developed for use on the high-altitude Large Altazimuth Telescope (LAT). The choice of the center frequency 90 GHz

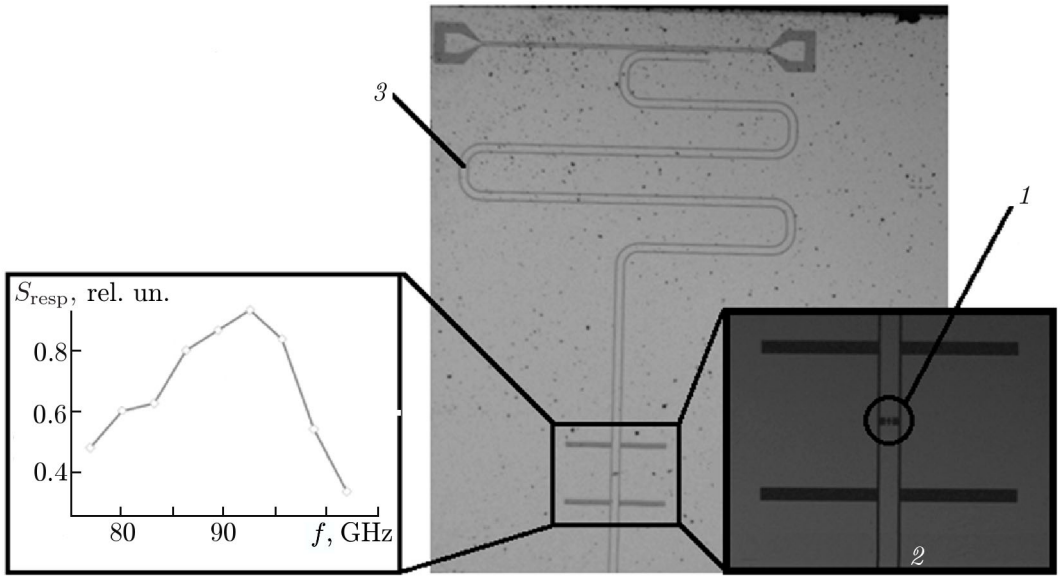

Fig. 11. SINIS detector *1* integrated into a double-slot antenna *2* of a frequency range in the vicinity of 90 GHz with microwave readout [92] (*3* is the quarter-wave resonator).

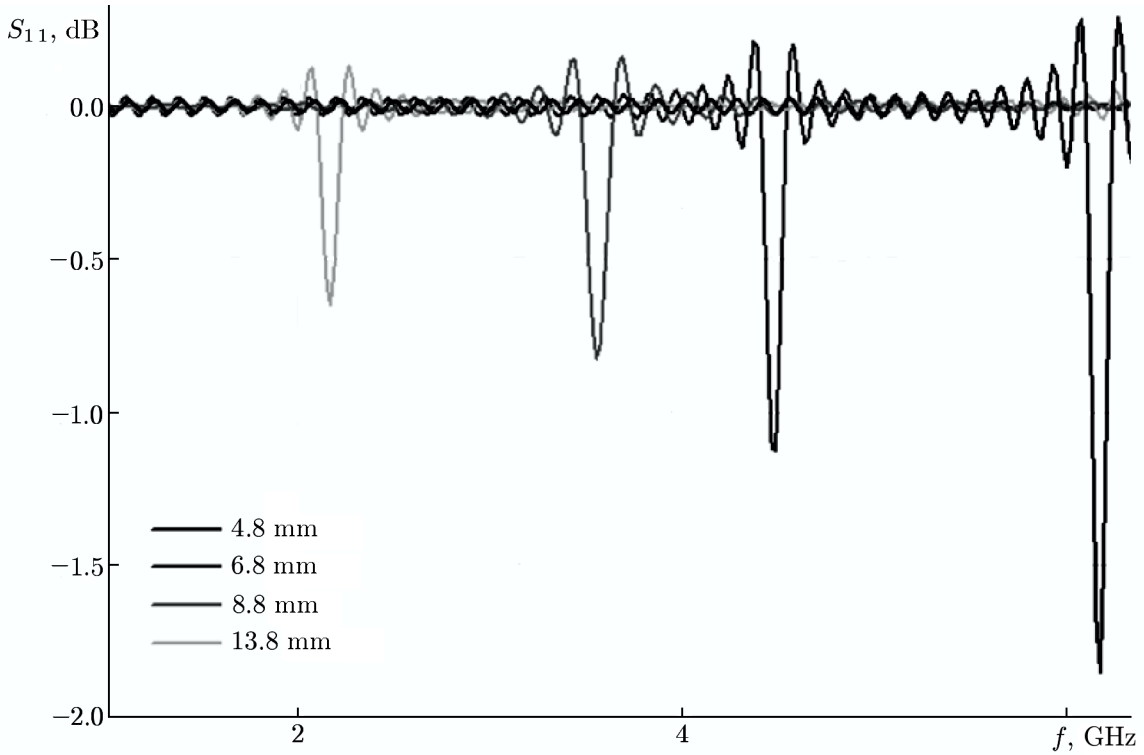

Fig. 12. Calculated S_{11} parameters for structures with different coplanar resonator lengths (load resistance 50 kΩ).

is due to the fact that the ground-based LAT telescope is supposed to be the first test site for the developed structures [66], and the atmospheric transparency at frequencies above 100 GHz is much worse in this case. The obtained results will be used to develop a prototype receiving system for the telescope under construction on the Suffa plateau [136] and in the future for the Russian Millimetron space observatory [137].

The resonator was made of a layer of superconducting NbN film with a thickness of 50 nm and a calculated kinetic inductance of 4 pH per square. This reduces drastically the geometric length of the

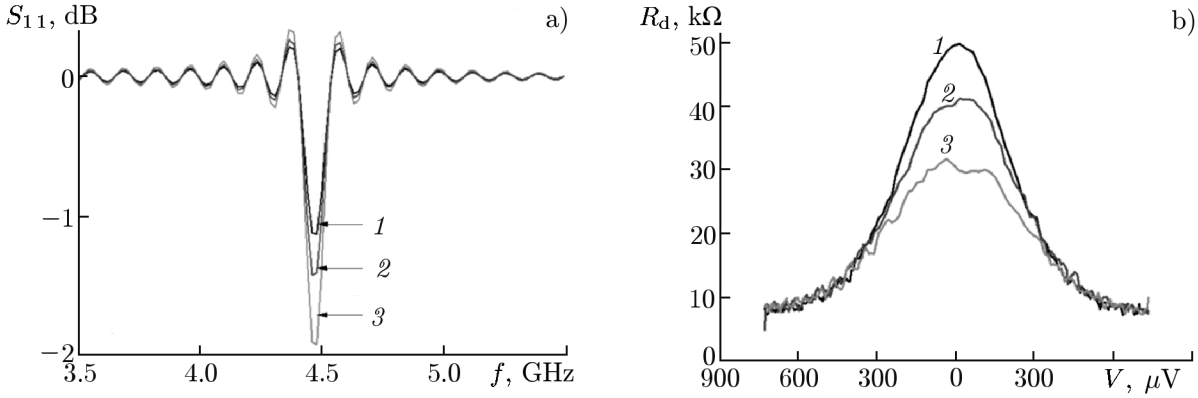

Fig. 13. (*a*) Calculated S_{11} parameters for structures with a coplanar resonator length of 6.8 mm at different load resistances: 50 kΩ (curve *1*), 40 kΩ (*2*), and 30 kΩ (*3*). (*b*) Differential resistance R_d at three signal power values corresponding to the source temperatures 3 (curve *1*), 6 (*2*), and 9 K (*3*) as a function of the bias voltage.

resonator. The bolometers were formed in the second layer using a two-layer resistive mask followed by sputtering at the angles of the superconducting aluminum electrodes. Normal metal is aluminum with a thickness of 14 nm, whose superconductivity is suppressed by the underlying iron film with a thickness of 1.2 nm. The barrier was formed during the oxidation of this Fe/Al layer.

The measurements were made in a modified Oxford Instruments Heliox AC-V cryostat at a temperature of 300 mK. The spectral response of the test sample was measured using a frequency-tunable source based on a BWO in the range 75–100 GHz (Fig. 11, left). The radiation power was normalized to the signal of the reference channel with a pyroelectric receiver.

The response of the sample to blackbody radiation at temperatures of 3, 6, and 9 K in an immersion cryostat of dissolution at a temperature of 100 mK was also measured [138]. The maximum of the differential resistance at a zero constant bias varies from 50 to 30 kΩ. The experimentally measured values of the differential resistance at three levels of radiation power are shown in Fig. 13. For a coplanar line with a resistance of 50 Ω, such a load corresponds to Q-factors 1000 and 300 for dark and irradiated cases, respectively. An impedance variation from 30 to 50 kΩ is easily detected by the Q-factor variation (calculated S_{11} parameters are shown in Fig. 13*a*) and permits frequency-separated channel readout.

7. CONCLUSIONS

In recent decades, there has been a rapid development of sub-terahertz astronomy, previously unknown unique data about the Universe have been obtained, more and more new problems based on these data are being posed, sub-terahertz wave telescopes are being built, and receiving systems for this research are being created. The team of authors of this publication working in close collaboration with the world community of astronomers and engineers, has also achieved significant results in this area in recent years, which are presented in this paper. A 211–275 GHz SIS mixer has been developed, manufactured, and studied; the experimentally measured receiver noise temperature (without corrections for losses in the beam splitter and the cryostat input window) is only two times higher than the hf/k_B quantum limit. The receivers under development can be used for the equipment of a number of ground-based radio telescopes (Suffa, ALMA, etc.), as well as for the Millimetron space program. The concept of a superconducting integrated receiver with a heterodyne oscillator based on a distributed Josephson junction has been developed and tested. A 450–650 GHz spectrometer has been successfully used to monitor the Earth's atmosphere. SIS mixers of the 800–950 GHz range with a noise temperature of 210 to 350 K were manufactured and explored, and a receiver with waveguide band separation at such a high frequency was created on their basis for the first time. SINIS detectors operated in the 90–400 GHz range with a volt–watt sensitivity of up to 10^9 V/W,

and a noise equivalent power of less than 10^{-16} W/Hz$^{1/2}$ have been developed and examined.

Progress in the presented developments could be much greater if there were sub-terahertz wave telescopes in Russia. In this regard, it should only be mentioned that the very edge of the low-frequency part of this range is occupied by the RT-22 radio telescope of the Crimean Astrophysical Laboratory and RATAN-600 (but their efficiency is not very high), and there are also exotic plans presented above for using the LAT optical telescope in the sub-terahertz range. In fact, in Russia, only one of the two 7-meter antennas of the Bauman Moscow State University near Dmitrov worked in a range of down to submillimeter waves; moreover, the Moscow region astroclimate actually does not give a chance to observe space objects at sub-terahertz waves, and the mirror size, limited to 7 m, does not promise breakthrough results. There is no doubt that the long-awaited attainment of the stage of practical use of two long-standing national projects Suffa and Millimetron, which are already the main motivators for the team of authors of this paper, will give an undisputable impetus to the above developments.

It is also extremely expedient to organize in Russia a large complex infrastructure project "sub-terahertz astronomy," which was initiated by the Russian Academy of Sciences and the main participants of which are the SAO RAS, which has already two instruments (LAT and RATAN-600) where the equipment and methods of sub-terahertz observations can be worked out, and qualified personnel, Astrospace Center of the Lebedev Physical Institute, already leading two basic projects for the development of sub-terahertz astronomy (Millimetron and Suffa), with the participation of the Kotelnikov IRE RAS, IAP RAS, and other universities and research institutes that already have, like the representatives of the Nizhny Novgorod school of radiophysics, a substantial foundation that can be used in the project. As a result of such a project, it would be possible not only to solve some of the scientific problems outlined in the paper, but also build the first sub-terahertz telescope in Russia, as well as to create and develop a national base for sub-terahertz instrumentation, which has also the best prospects outside the field of astronomy.

The work is dedicated to the memory of the recently deceased teacher and a remarkable scientist A. G. Kislyakov, one of the pioneers of the development of the millimeter and submillimeter wavelength ranges in astronomy and astronomical instrumentation, and Honored Professor of the Radiophysics Faculty at the N. I. Lobachevsky State University of Nizhny Novgorod.

This work was supported by the State Assignment of the Kotelnikov IRE RAS (project No. 0030–2019–0003) and the IAP RAS (project No. 0035–2019–0005). The study of the SIS receivers was supported by the Russian Science Foundation (project No. 19–19–00618). The development of elements of the terahertz detector technology, as well as the creation of individual devices and elements of experimental tools for a study of the created structures, were performed within project No. 19-19-00499 of the Russian Science Foundation. The structures were manufactured on the basis of the technological section of the Kotelnikov IRE RAS using large-scale research facility 352529. Part of the process fine-tuning and sample production was carried out on the basis of the Swedish Micro- and Nanotechnology Consortium (Myfab) and supported by the Vetenskapsrådet project (No. 2016–05256) and the Knut and Alice Wallenberg Foundation.

REFERENCES

1. The Event Horizon Telescope Collaboration, *Astrophys. J. Lett.*, **875**, No. 1, L1 (2019). https://doi.org/10.3847/2041-8213/ab0ec7
2. The Event Horizon Telescope Collaboration, *Astrophys. J. Lett.*, **875**, No. 1, L2 (2019). https://doi.org/10.3847/2041-8213/ab0c96
3. A. G. Kislyakov, *Sov. Phys. Usp.*, **13**, 495–521 (1971). https://doi.org/10.1070/PU1971v013n04ABEH004683
4. A. G. Kislyakov, *Radiophys. Quantum Electron.*, **4**, No. 3, 433–443 (1961).

5. A. G. Kislyakov, A. D. Kuzmin, and A. E. Salomonovich, *Izv. Vyssh. Uchebn. Zaved. Radiofiz.*, **4**, No. 3, 573–574 (1961).
6. A. G. Kislyakov, and A. I. Naumov, *Sov. Astron., A.J.*, **11**, 1059–1060 (1968).
7. A. G. Kislyakov, *Izv. Vyssh. Uchebn. Zaved. Radiofiz.*, **1**, No. 4, 81–89 (1958).
8. Y. A. Dryagin, and L. I. Fedoseev, *Radiophys. Quantum Electron.*, **12**, No. 6, 647–691 (1969). https://doi.org/10.1007/BF01031242
9. V. A. Efanov, A. G. Kislyakov, I. G. Moiseev, and A. I. Naumov, *Astron. Zh.*, **46**, No. 1, 147–151 (1969).
10. A. G. Kislyakov, V. I. Chernyshov, Y. V. Lebsky, et al., *Astron. Zh.*, **48**, No. 1, 39–45 (1971).
11. A. M. Belyantsev, and V. N. Genkin, *Radiophys. Quantum Electron.*, **12**, No. 5, 609–611 (1969). https://doi.org/10.1007/BF01033144
12. A. G. Kislyakov, Y. V. Lebsky, and A. I. Naumov, *Radiophys. Quantum Electron.*, **11**, No. 12, 1001–1006 (1968). https://doi.org/10.1007/BF01032962
13. http://lmtgtm.org
14. https://pole.uchicago.edu
15. http://olimpo.roma1.infn.it
16. https://www.cosmos.esa.int/web/planck
17. http://millimetron.ru/index.php/en/
18. A. G. Kislyakov, V. A. Razin, and N. M. Tseitlin, *Introduction to Radio Astronomy, Part 2, Radio Astronomy Technique (textbook for universities)* [in Russian], N. I. Lobachevsky State University of Nizhny Novgorod, Nizhny Novgorod (1996), p. 23.
19. I. I. Zinchenko, A. M. Baryshev, and V. F. Vdovin, *Astron. Lett.*, **23**, No. 2, 123–126 (1997).
20. V. F. Vdovin, A. I. Eliseev, I. I. Zinchenko, et al., *J. Commun. Technol. Electron.*, **50**, No. 9, 1118–1122 (2005).
21. V. Vdovin, O. Bolshakov, J. Kalunki, et al., in: *The X Finnish-Russian Radio Astronomy Symposium, 1–5 September, 2008, Orilampi, Finland*, http://citeseerx.ist.psu.edu/viewdoc/download?doi=10.1.1.557.7590&rep=rep1&type=pdf
22. J. R. Tucker, and M. J. Feldman, *Rev. Mod. Phys.*, **57**, No. 4, 1055–1113 (1985). https://doi.org/10.1103/RevModPhys.57.1055
23. A. R. Kerr, *IEEE Trans. Microw. Theory Tech.*, **47**, No. 3, 325–329 (1999). https://doi.org/10.1109/22.750234
24. J. W. Kooi, M. Chan, T. G. Phillips, et al., *IEEE Trans. Microw. Theory Tech.*, **40**, No. 5, 812–815 (1992). https://doi.org/10.1109/22.137383
25. A. Karpov, J. Blondell, M. Voss, and K. H. Gundlach, *IEEE Trans. Appl. Supercond.*, **5**, No. 2, 3304–3307 (1995). https://doi.org/10.1109/77.403298
26. B. D. Jackson, G. de Lange, T. Zijlstra, et al., *IEEE Trans. Microw. Theory Tech.*, **54**, No. 2, 547–558 (2006). https://doi.org/10.1109/TMTT.2005.862717
27. A. Karpov, D. Miller, F. Rice, et al., *IEEE Trans. Appl. Supercond.*, **17**, No. 2, 343–346 (2007). https://doi.org/10.1109/TASC.2007.898277
28. A. R. Kerr, S-K. Pan, S. M. X. Claude, et al., *IEEE Trans. Terahertz Sci. Technol.*, **4**, No. 2, 201–212 (2014). https://doi.org/10.1109/TTHZ.2014.2302537
29. A. M. Baryshev, R. Hesper, F. P. Mena, et al., *Astron. Astrophys.*, **577**, A129 (2015). https://doi.org/10.1051/0004-6361/201425529

30. Y. Uzawa, Y. Fujii, A. Gonzalez, et al., *IEEE Trans. Appl. Supercond.*, **25**, No. 3, 2401005 (2014). https://doi.org/10.1109/TASC.2014.2386211

31. A. Khudchenko, A. M. Baryshev, K. Rudakov, et al., *IEEE Trans. Terahertz Sci. Technol.*, **6**, No. 1, 127–132 (2016). https://doi.org/10.1109/TTHZ.2015.2504783

32. Th. de Graauw, F. P. Helmich, T. G. Phillips, et al., *Astron. Astrophys.*, **518**, L6 (2010). https://doi.org/10.1051/0004-6361/201014698

33. A. Karpov, J. A. K. Blondel, K. H. Gundlach, and D. Billion-Pierron, *J. Infrared Millim. Terahertz Waves*, **18**, 301–317 (1997). https://doi.org/10.1007/BF02677922

34. https://www.almaobservatory.org/en/audience/science/

35. https://www.almaobservatory.org/en/about-alma-at-first-glance/how-alma-works/technologies/receivers/

36. A. V. Smirnov, A. M. Baryshev, P. de Bernardis, et al., *Radiophys. Quantum Electron.*, **54**, Nos. 8–9, 557–568 (2011). https://doi.org/10.1007/s11141-012-9314-z

37. C. E. Groppi and J. H. Kawamura, *IEEE Trans. Terahertz Sci. Technol.*, **1**, No. 1, 85–96 (2011). https://doi.org/10.1109/TTHZ.2011.2159555

38. P. F. Goldsmith, *URSI Radio Sci. Bull.*, **2017**, No. 362, 53–73 (2017). https://doi.org/10.23919/URSIRSB.2017.8267373

39. T. Kojima, M. Kroug, A. Gonzalez, et al., *IEEE Trans. Terahertz Sci. Technol.*, **8**, No. 6, 638–646 (2018). https://doi.org/10.1109/TTHZ.2018.2873487

40. T. Kojima, H. Kiuchi, K. Uemizu, et al., *Astron. Astrophys.*, **640**, L9 (2020). https://doi.org/10.1051/0004-6361/202038713

41. R. Hesper, A. Khudchenko, A. M. Baryshev, et al., *IEEE Trans. Terahertz Sci. Technol.*, **7**, No. 6, 686–693 (2017). https://doi.org/10.1109/TTHZ.2017.2758270

42. A. Khudchenko, R. Hesper, A. M. Baryshev, et al., *IEEE Trans. Terahertz Sci. Technol.*, **9**, No. 6, 532–539 (2019). https://doi.org/10.1109/TTHZ.2019.2939003

43. F. Giazotto, T. T. Heikkilä, A. Luukanen, et al., *Rev. Mod. Phys.*, **78**, No. 1, 217–274 (2006). https://doi.org/10.1103/RevModPhys.78.217

44. J. N. Ullom, *AIP Conf. Proc.*, **605**, 135–140 (2002). https://doi.org/10.1063/1.1457613

45. M. Tarasov and V. Edelman, in: A. Sidorenko, ed., *Functional Nanostructures and Metamaterials for Superconducting Spintronics. Nanoscience and Technology*, Springer, Cham (2018), p. 91–116. https://doi.org/10.1007/978-3-319-90481-8_5

46. A. V. Feshchenko, L. Casparis, I. M. Khaymovich, et al., *Phys. Rev. Appl.*, **4**, No. 3, 034001 (2015). https://doi.org/10.1103/physrevapplied.4.034001

47. J. Pekola, *J. Low Temperature Phys.*, **135**, Nos. 5–6, 723–744 (2004). https://doi.org/10.1023/b:jolt.0000029516.18146.42

48. E. Isosaari, T. Holmqvist, M. Meschke, et al., *The European Phys. J. Special Topics*, **172**, No. 1, 323–332 (2009). https://doi.org/10.1140/epjst/e2009-01057-y

49. J. P. Pekola, A. J. Manninen, M. M. Leivo, et al., *Phys. B*, **280**, Nos. 1–4, 485–490 (2000). https://doi.org/10.1016/S0921-4526(99)01842-6

50. H. Q. Nguyen, T. Aref, V. J. Kauppila, et al., *New J. Phys.*, **15**, No. 8, 085013 (2013). https://doi.org/10.1088/1367-2630/15/8/085013

51. A. M. Clark, N. A. Miller, A. Williams, et al., *Appl. Phys. Lett.*, **86**, No. 17, 173508 (2005). https://doi.org/10.1063/1.1914966

52. G. C. O'Neil, *Improving NIS Tunnel Junction Refrigerators: Modeling, Materials, and Traps: A thesis for the degree of Doctor of Physics,* University of Colorado, Boulder (2011).

53. M. Nahum and J. M. Martinis, *Appl. Phys. Lett.*, **63**, No. 22, 3075–3077 (1993). https://doi.org/10.1063/1.110237

54. M. Nahum, P. L. Richards, and C. A˙ Mears, *IEEE Trans. Appl. Supercond.*, **3**, No. 1, 2124–2127 (1993). https://doi.org/10.1109/77.233921

55. A. Vystavkin, D. Shuvaev, L. Kuzmin, and M. Tarasov, *J. Exp. Theor. Phys.*, **88**, No. 3, 598–602 (1999). https://doi.org/10.1134/1.558834

56. L. Kuzmin, I. Devyatov, and D. Golubev, *Proc. SPIE*, **3465**, 193–199 (1998). https://doi.org/10.1117/12.331165

57. T. L. R. Brien, P. A. R. Ade, P. S. Barry, et al., *Appl. Phys. Lett.*, **105**, No. 4, 043509 (2014). https://doi.org/10.1063/1.4892069

58. D. R. Schmidt, W. D. Duncan, K. D. Irwin, et al., *Nucl. Instrum. Methods Phys. Res.*, **559**, No. 2, 516–518 (2006). htpps://doi.org/10.1016/j.nima.2005.12.043

59. D. R. Schmidt, K. W. Lehnert, A. M. Clark, et al., *Appl. Phys. Lett.*, **86**, No. 5, 053505 (2005). https://doi.org/10.1063/1.1855411

60. I. A. Devyatov, P. A. Krutitskiy, and M. Y. Kupriyanov, *JETP Lett.*, **84**, No. 2, 57–61 (2006). https://doi.org/10.1134/S0021364006140037

61. I. A. Devyatov and M. Y. Kupriyanov, *JETP Lett.*, **80**, No. 10, 646–650 (2004). https://doi.org/10.1134/1.1857272

62. M. Tarasov, V. Edelman, S. Mahashabde, et al., *Appl. Phys. Lett.*, **110**, No. 24, 242601 (2017). https://doi.org/10.1063/1.4986463

63. R. A. Yusupov, A. A. Gunbina, A. M. Chekushkin, et al., *Phys. Solid State*, **62**, No. 9, 1567–1570 (2020). https://doi.org/10.1134/S106378342009036X

64. A. A. Gunbina, S. A. Lemzyakov, M. A. Tarasov, et al., *JETP Lett.*, **111**, No. 10, 539–542 (2020). https://doi.org/10.1134/S0021364020100094

65. A. M. Chekushkin, M. A. Tarasov, R. A. Yusupov, et al., *Trudy MFTI*, **10**, No. 2, 64–71 (2018).

66. http://w0.sao.ru/hq/sekbta/

67. G. Yakopov, M. Tarasov, A. Gunbina, et al., *EPJ Web Conf.*, **195**, 05014 (2018). https://doi.org/10.1051/epjconf/201819505014

68. I. I. Zinchenko, *Radiophys. Quantum Electron.*, **46**, Nos. 8–9, 577–593 (2003). https://doi.org/10.1023/B:RAQE.0000024989.12653.a0

69. N. S. Kardashev, I. D. Novikov, V. N. Lukash, et al., *Phys.-Usp.*, **57**, No. 12, 1199–1228 (2014). https://doi.org/10.3367/UFNe.0184.201412c.1319

70. V. K. Dubrovich, *Sov. Astron. Lett.*, **3**, 128–129 (1997).

71. V. K. Dubrovich and A. A. Lipovka, *Astron. Astrophys.*, **296**, 307–309 (1995).

72. V. K. Dubrovich, *Astron. Astrophys.*, **324**, No. 1, 27–31 (1997).

73. D. Galli and F. Palla, *Annu. Rev. Astron. Astrophys.*, **51**, 163–206 (2013). https://doi.org/10.1146/annurev-astro-082812-141029

74. R. Güsten, H. Wiesemeyer, D. Neufeld, et al., *Nature.*, **568**, No. 7752, 357–359 (2019). https://doi.org/10.1038/s41586-019-1090-x

75. I. Zinchenko, V. Dubrovich, and C. Henkel, *Mon. Not. R. Astron. Soc.*, **415**, No. 1, L78–L80 (2011). https://doi.org/10.1111/j.1745-3933.2011.01083.x

76. I. D. Novikov, S. F. Likhachev, U. A. Shekinov, et al., *Phys. Usp.*, **64**, No. 4. https://doi.org/10.3367/UFNe.2020.12.038898

77. M. Kamionkowski and E. D. Kovetz, *Ann. Rev. Astron. Astrophys.*, **54**, 227–269 (2016). https://doi.org/10.1146/annurev-astro-081915-023433

78. P. A. R. Ade, M. Aguilar, et al., *Astrophys. J.*, **848**, No. 2, 121–136 (2017). https://doi.org/10.3847/1538-4357/aa8e9f

79. https://www.cosmos.esa.int/web/planck

80. V. K. Dubrovich and S. I. Grachev, *Astron. Lett.*, **41**, No. 10, 537–548 (2015). https://doi.org/10.1134/S1063773715100023

81. V. K. Dubrovich and S. I. Grachev, *Astron. Lett.*, **42**, No. 11, 713–720 (2016). https://doi.org/10.1134/S1063773716110025

82. V. K. Dubrovich, S. I. Grachev, and V. G. Romanuk, *Astron. Lett.*, **35**, No. 11, 723–729 (2009). https://doi.org/10.1134/S1063773709110012

83. V. K. Dubrovich and S. I. Grachev, *Astron. Lett.*, **44**, No. 4, 213–219 (2018). https://doi.org/10.1134/S1063773718040011

84. V. Dubrovich, S. Grachev, and T. Zalialiutdinov, *Astron. Astrophys.*, **619**, A29 (2018). https://doi.org/10.1051/0004-6361/201833554

85. V. K. Dubrovich, *Astron. Lett.*, **29**, No. 1, 6–9 (2003). https://doi.org/10.1134/1.1537371

86. S. I. Grachev and V. K. Dubrovich, *Astron. Lett.*, **37**, No. 5, 293–301 (2011). https://doi.org/10.1134/S1063773711040013

87. https://www.jwst.nasa.gov

88. P. V. Shcheglov, *Problems of Optical Astronomy* [in Russian], Nauka, Moscow (1980).

89. A. G. Kislyakov and K. S. Stankevich, *Radiophys. Quantum Electron.*, **10**, Nos. 9–10, 695–708 (1967). https://doi.org/10.1007/BF01031599

90. V. I. Nosov, O. S. Bol'shakov, G. M. Bubnov, et al., *Inst. Exp. Tech.*, **59**, No. 3, 374–380 (2016). https://doi.org/10.1134/S0020441216020111

91. G. M. Bubnov, V. F. Vdovin, V. Yu. Bukov, et al., in: *32nd URSI GASS, 19–26 August 2017, Montreal*, 8105000. https://doi.org/10.23919/URSIGASS.2017.8105000

92. G. M. Bubnov and P. M. Zemlyanukha, "Computer program 2019664403 RF. Data processing program for atmospheric transparency in the millimeter wavelength range" [in Russian], No. 2019663109, claimed: October 15, 2019, published: November 6, 2019.

93. G. M. Bubnov, V. F. Grigorev, V. F. Vdovin, et al., in: em 30th Int. Symp. Space THz Technol. (ISSTT2019), 15–17 April 2019, Gothenburg, Sweden, p. 143–148.

94. H. J. Liebe, P. W. Rosenkranz, and G. A. Hufford, *J. Quant. Spectrosc. Radiat. Transf.*, **48**, Nos. 5–6, 629–643 (1992). https://doi.org/10.1016/0022-4073(92)90127-P

95. L. S. Rothman, I. E. Gordon, Y. Babikov, et al., *J. Quant. Spectrosc. Radiat. Transf.*, **130**, 4–50 (2013). https://doi.org/10.1016/j.jqsrt.2013.07.002

96. N. Jacquinet-Husson, L. Crepeau, R. Armante, et al., *J. Quant. Spectrosc. Radiat. Transf.*, **112**, No. 15, 2395–2445 (2011). https://doi.org/10.1016/j.jqsrt.2011.06.004

97. S. V. Shytov, V. F. Vdovin, I. I. Zinchenko, et al., "Test of the radiometer with a SIS mixer at the RT-25*2 radio telescope" [in Russian], preprint No. 309, Inst. Appl. Phys. Rus. Acad. Sci., Nizhny Novgorod (1992).

98. Y. N. Artemenko, Y. Yu. Balega, A. M. Baryshev, et al., in: *ISSTT2019, 15–17 April 2019, Gothenburg, Sweden*, p. 196–201.

99. K. I. Rudakov, P. N. Dmitriev, A. M. Baryshev, et al., *Radiophys. Quantum Electron.*, **62**, Nos. 7–8, 547–555 (2019). https://doi.org/10.1007/s11141-020-10001-7

100. J. R. Tucker, *IEEE J. Quantum Electron.*, **15**, No. 11, 1234–1258 (1979). https://doi.org/10.1109/JQE.1979.1069931

101. V. P. Koshelets and S. V. Shitov, *Supercond. Sci. Technol.*, **13**, No. 5, R53–R59 (2000). https://doi.org/10.1088/0953-2048/13/5/201

102. V. P. Koshelets, P. N. Dmitriev, A. B. Ermakov, et al., *Radiophys. Quantum Electron.*, **48**, No. 10–11, 844–850 (2005). https://doi.org/10.1007/s11141-006-0016-2

103. V. P. Koshelets, L. V. Filipenko, V. B. Borisov, et al., *Radiophys. Quantum Electon.*, **50**, Nos. 10–11, 847–851 (2007). https://doi.org/10.1007/s11141-007-0076-y

104. G. de Lange, M. Birk, D. Boersma, et al., *Supercond. Sci. Technol.*, **23**, No. 4, 045016 (2010). https://doi.org/10.1088/0953-2048/23/4/045016

105. A. de Lange, M. Birk, G. de Lange, et al., *Atmos. Meas. Tech.*, **5**, 487–500 (2012). https://doi.org/10.5194/amt-5-487-2012

106. V. P. Koshelets, P. N. Dmitriev, M. I. Faley, et al., *IEEE Trans. Terahertz Sci. Technol.*, **5**, No. 4, 687–694 (2015). https://doi.org/10.1109/TTHZ.2015.2443500

107. P. N. Dmitriev, L. V. Filippenko, and V. P. Koshelets, in: E. L. Wolf, G. B. Arnold, M. A. Gurvitch, and J. F. Zasadzinski, eds., *Josephson Junctions: History, Devices, and Applications*, Pan Stanford Publishing Pte. Ltd., Singapore (2017), p. 185–244.

108. M. Li, J. Yuan, N. Kinev, et al., *Phys. Rev. B*, **86**, 060505 (2012). https://doi.org/10.1103/PhysRevB.86.060505

109. N. V. Kinev, L. V. Filippenko, M. Y. Li, et al., *Radiophys. Quantum Electron.*, **56**, Nos. 8–9, 582–590 (2013). https://doi.org/10.1007/s11141-014-9462-4

110. A. Wootten and A. R. Thompson, *Proc. IEEE*, **97**, No. 8, 1463–1471 (2009). https://doi.org/10.1109/JPROC.2009.2020572

111. R. Gusten, R. S. Booth, C. Cesarsky, et al., *Proc. SPIE*, **6267**, 626714 (2006). https://doi.org/10.1117/12.670798

112. K. I. Rudakov, V. P. Koshelets, A. M. Baryshev, et al., *Radiophys. Quantum Electron.*, **59**, Nos. 8–9, 711–714 (2017). https://doi.org/10.1007/s11141-017-9739-5

113. V. Y. Belitsky, S. W. Jacobsson, L. V. Filippenko, and E. L. Kollberg, *Microw. Opt. Technol. Lett.*, **10**, No. 2, 74–78 (1995). https://doi.org/10.1002/mop.4650100203

114. A. M. Belyantsev and E. V. Klishin, *Radiophys. Quantum Electron.*, **16**, No. 3, 363–364 (1973). https://doi.org/10.1007/BF01032373

115. P. K. Day, H. G. LeDuc, B. A. Mazin, et al., *Nature*, **425**, 817–821 (2003). https://doi.org/10.1038/nature02037

116. A. V. Sergeev, V. V. Mitin, and B. S. Karasik, *Appl. Phys. Lett.*, **80**, No. 5, 817–819 (2002). https://doi.org/10.1063/1.1445462

117. S. Doyle, P. Mauskopf, J. Naylon, et al., *J. Low Temperature Phys.*, **151**, 530–536 (2008). https://doi.org/10.1007/s10909-007-9685-2

118. M. R. Vissers, J. E. Austermann, M. Malnou, et al., *Appl. Phys. Lett.*, **116**, No. 3, 032601 (2020). https://doi.org/10.1063/1.5138122

119. A. Wandui, J. Bock, C. Frez, et al., *J. Appl. Phys.*, **128**, 044508 (2020). https://doi.org/10.1063/5.0002413

120. A. Paiella, P. A. R. Ade, E. S. Battistelli, et al., *J. Low Temp. Phys.*, **199**, 491–501 (2020). https://doi.org/10.1007/s10909-020-02372-y

121. P. Day, H. G. Leduc, C. D. Dowell, et al., *J. Low Temp. Phys.*, **151**, 477–482 (2008). https://doi.org/10.1007/s10909-007-9676-3

122. W. S. Holland, D. Bintley, E. L. Chapin, et al., *Mon. Not. R. Astron. Soc.*, **430**, No. 4, 2513–2533 (2013). https://doi.org/10.1093/mnras/sts612

123. J. A. Bonetti, A. D. Turner, M. Kenyon, et al., *IEEE Trans. Appl. Supercond.*, **21**, No. 3, 219–222 (2011). https://doi.org/10.1109/TASC.2010.2093858

124. G. C. Jaehnig, K. Arnold, J. Austermann, etal., *J. Low Temperature Phys.*, **199**, 646–653 (2020). https://doi.org/10.1007/s10909-020-02425-2

125. A. D. Semenov, G. N. Gol'tsman, and R. Sobolewski, *Supercond. Sci. Technol.*, **15**, No. 4, R1–R16 (2002). https://doi.org/10.1088/0953-2048/15/4/201

126. G. Yakopov, M. Tarasov, A. Gunbina, et al., *EPJ Web Conf.*, **195**, 05014 (2018). https://doi.org/10.1051/epjconf/201819505014

127. M. A. Tarasov, A. A. Gunbina, S. Mahashabde, et al., *IEEE Trans. Appl. Supercond.*, **30**, No. 3, 2300106 (2020). https://doi.org/10.1109/TASC.2019.2941857

128. S. Mahashabde, A. Sobolev, A. Bengtsson, et al., *IEEE Trans. Terahertz Sci. Technol.*, **5**, No. 1, 145–152 (2015). https://doi.org/10.1109/TTHZ.2014.2362010

129. S. Mahashabde, A. Sobolev, M. A. Tarasov, and L. S. Kuzmin, *IEEE Trans. Terahertz Sci. Technol.*, **5**, No. 1, 37–43 (2015). https://doi.org/10.1109/TTHZ.2014.2377247

130. M. Tarasov, A. Sobolev, A. Gunbina, et al., *J. Appl. Phys.*, **THZ2019**, No. 1, 174501 (2019). https://doi.org/10.1063/1.5054160@jap.2019.THZ2019.issue-1

131. M. A. Tarasov, A. S. Sobolev, A. M. Chekushkin, R. A. Yusupov, and A. A. Gunbina, Patent No. 2684897 RF, IPC G01J 5/02 (2006.01), "Wideband terahertz detector No. 2018124492" [in Russian], claimed: July 4, 2018, published: April 16, 2019, IRE RAS.

132. A. A. Gunbina, M. A. Tarasov, S. A. Lemzyakov, et al., *Phys. Solid State*, **62**, No. 9, 1604-1611 (2020). https://doi.org/10.1134/S1063783420090097

133. M. Abitbol, Z. Ahmed, D. Barron, et al., https://arxiv.org/abs/1706.02464

134. L. Ferrari, O. Yurduseven, N. Llombart, et al., *IEEE Trans. Terahertz Sci. Technol.*, **8**, No. 1, 127–139 (2017). https://doi.org/10.1109/TTHZ.2017.2764378

135. M. A. Tarasov, S. Makhashabde, A. A. Gunbina, et al., *Phys. Solid State*, **62**, No. 9, 1580-1584 (2020). https://doi.org/10.1134/S1063783420090292

136. http://www.ipme.ru/ipme/labs/RT-70/source/start.html

137. http://www.asc.rssi.ru/millimetron/millim.html

138. V. S. Edel'man, *Instrum. Exp. Tech.*, **52**, No. 2, 301–307 (2009). https://doi.org/10.1134/S002044120902033X